Delft University of Technology

Point contact abrasive wear behavior of MAX phase materials

Qu, Lianshi; Bei, Guoping; Nijemeisland, Marlies; Cao, Dianxue; van der Zwaag, Sybrand; Sloof, Willem G.

Important note
To cite this publication, please use the final published version (if applicable).
Please check the document version above.

Point contact abrasive wear behavior of MAX phase materials

Lianshi Qu[a,b], Guoping Bei[b,*], Marlies Nijemeisland[c], Dianxue Cao[a], Sybrand van der Zwaag[c], Willem G. Sloof[b]

[a] *College of Materials Science and Chemical Engineering, Harbin Engineering University, Harbin, 15001, China*
[b] *Delft University of Technology, Department of Materials Science and Engineering, Delft, Mekelweg 2, 2628 CD, Delft, the Netherlands*
[c] *Delft University of Technology, Faculty Aerospace Engineering, Kluyverweg 1, 2629 HS, Delft, the Netherlands*

ARTICLE INFO

ABSTRACT

The room temperature abrasive wear behavior of three selected MAX phases, Ti_3SiC_2, solution strengthened $Ti_{2.7}Zr_{0.3}SiC_2$ and Cr_2AlC, is investigated by low velocity scratch testing using a diamond conical indentor with a final radius of 100 μm and a cone angle of 120° and applied loads of up to 20 N. All three materials showed a relatively low wear resistance in comparison to most engineering ceramics such as Al_2O_3, Si_3N_4 and SiC. For all three materials, the wear rate scaled more or less linearly with the applied load. The softer Ti_3SiC_2 with a hardness of 2.8 GPa showed the lowest wear resistance with extensive ploughing and grain breakout damage, both within and outside the direct wear track, in particular at the highest load. The hardest material, $Ti_{2.7}Zr_{0.3}SiC_2$, with a hardness of 7.3 GPa, showed a 5 times better wear resistance. The Cr_2AlC with a hardness of 4.8 GPa showed a wear resistance equal to or even better than that of the $Ti_{2.7}Zr_{0.3}SiC_2$. The wear mechanism depends on the applied load and the microstructure of the MAX phase materials tested. For the Ti_3SiC_2 sample, a quasi-plastic deformation behavior occurs below a point load of 10 N, resulting in grain bending, kink band formation and delamination, grain de-cohesion, as well as trans-and intra-granular fracture near the scratch groove. At this load, the $Ti_{2.7}Zr_{0.3}SiC_2$ and Cr_2AlC MAX samples display plastic ploughing, grain boundary cracks and material dislodgments.

1. Introduction

Advanced engineering ceramics are being used extensively in demanding wear resistant components due to their unique combination of desirable properties such as high hardness and strength, good wear resistance and exceptional stability [1–3]. They perform well as sliding components in a variety of engineering applications including engine components like bearings, rollers, dies, tappets, valves, fuel injectors, but also biomechanical components, like dental restorations and hip prostheses where contact, scratch and wear damage are critical factors for their performance [1–3]. However, a major drawback of engineering ceramics is their intrinsic brittleness and related machinability issues. To overcome these disadvantages, efforts have been made to enhance their toughness and reduce their damage sensitivity [2]. In addition, ceramic composites with crack-healing ability have been developed for high temperature applications to make them more robust and (contact-) damage resistant [4–6].

Recently, machinable nano-layered ternary ceramics denoted as $M_{n+1}AX_n$ phase (n = 1 to 3), where M is an early transition metal, A is

an A group element, and X is either carbon or nitrogen, have attracted quite some attention due to their unique crystal structure and unusual combination of ceramic and metallic-like properties [7,8]. These MAX phases have a hexagonal crystal lattice (space group $P6_3/mmc$) with an edge-sharing $[M_6X]$ octahedral interleaved by a layer of A atoms. In this nano-layered structure, the M and X atoms are connected by strong covalent bonds, while the M and A atoms are connected by weaker metallic bonds [7,8]. Most of these MAX phases possess a high thermal and electrical conductivity, are damage tolerant [9], and show self-lubrication [2,3]. In particular, MAX phases with Al and Si as A-element are oxidation resistant and exhibit crack healing abilities at higher temperatures in oxygen containing atmospheres [10–12]. Moreover, MAX phases are easy machinable. Therefore, MAX phases are considered as promising material for tribological applications. Hence, wear behavior or tribological properties of monolithic bulk MAX phase materials [13–18], MAX phase based composites [19–21], MAX phase coatings [22] have been investigated and reported in literatures. For example, under dry sliding conditions against a low carbon steel disk, the friction coefficient of $Ti_3Al(Sn)C_2$ could be tailored by incorporation

of different amounts of Sn in the Ti_3AlC_2 MAX phase [17]. The steady state friction coefficient could be tuned from a value of 0.1 to a value of 0.4 by tailoring the formation of self-adaptable friction film composed of Ti, Sn, Al and Fe oxides.

Provided the appropriate conditions are selected, single point scratch testing is an efficient way to evaluate the multi-body wear and damage behavior of materials since the indenter tip can be considered as a model of contact asperity and a variety of experimental parameters can be tested, such as: sliding speed, applied force, constant or progressive load, single or repeated scratching, etc. [23–27]. This technique offers the opportunity to study the material resistance at conditions mimicking either light or heavy abrasion. In the present work, single point scratch testing is utilized to examine the abrasion behavior of three selected MAX phases with different grades of purity and hardness, viz.: Ti_3SiC_2, $Ti_{2.7}Zr_{0.3}SiC_2$ and Cr_2AlC. The effect of the scratch load, phase composition and microstructure on the room temperature wear properties is evaluated.

2. Experimental details

The synthesis of the Ti_3SiC_2 and $Ti_{2.7}Zr_{0.3}SiC_2$ samples is described in detail elsewhere [28]. Briefly, a reactant mixture with a molar ratio of 1.0Ti-1.0Si-1.9TiC and 0.7Ti-0.3Zr-1.0Si-1.9TiC is homogeneously mixed and then loaded into a graphite die with an inner diameter of 20 mm and covered from both sides with graphite punches. Next, powder mixtures are Spark Plasma Sintered (SPS) in a SPS installation (HP D 25 SD, FCT system GmbH, Germany) for 1 h at temperatures ranging from 1450 to 1650 °C, respectively, under a pressure of 50 MPa. During the sintering process the furnace is flushed with pure Ar (5 N purity, Linde, The Netherlands) to minimize the risk of oxidation of the constituent phases. The heating and cooling rate was 50 °C/min.

For the synthesis of Cr_2AlC MAX phase, a reactant mixture of 2Cr-1.1Al-1.0C powder was prepared. To avoid leakage of unreacted liquid Al during sintering SPS processing, the pressure versus time profile was modified based on a large number of less successful experiments to obtain dense and pure materials. Prior to heating, the powder mixture is pre-pressed at 50 MPa for 5 min. Then, the pressure was reduced to 5 MPa and the heating was started. When reaching the sintering temperature of 1200 °C, it was held for 30 min at a pressure of 5 MPa. Next, the pressure was gradually increased up to 50 MPa within 10 min. Thereafter, the pressure of 50 MPa and the temperature of 1200 °C were maintained for another hour. The heating and cooling rate were set to 30 and 50 °C/min, respectively.

To prepare three materials for scratch testing, the samples were cut into small plates of $15 \times 8 \times 2 \, mm^3$ making sure that the samples were sufficiently far removed from the surfaces of the SPS produced samples. One of the cut sample surfaces was polished with SiC emery paper starting with 240 grit and finishing with 4000 grit. Finally, this surface was polished with 1 μm diamond grain suspension on a soft cloth.

For abrasion experiments, a computer controlled CSM micro-scratch tester (CSM-instruments, Switzerland) was used. A diamond Rockwell indenter with a tip radius of 100 μm and a cone angle of 120° was mounted on this scratch tester. The sliding speed was set at 1.5 mm/min and the scratch length was set to 3 mm. All tests were conducted at room temperature. The wear rate (W_r) of the MAX phases was calculated from following formula:
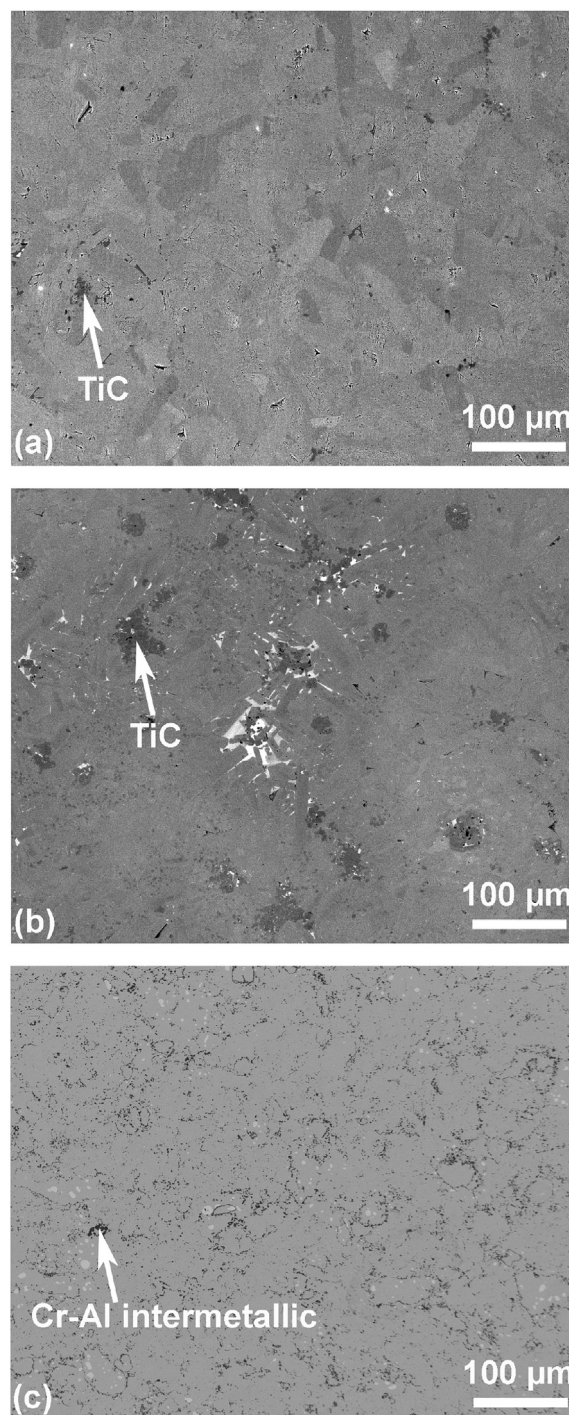

Fig. 1. Phase composition and microstructure of Cr_2AlC MAX phase material: (a) X-ray diffraction pattern, and (b) SEM backscattered electron image.

Table 1
Phase composition, grain size and hardness of MAX phase materials.

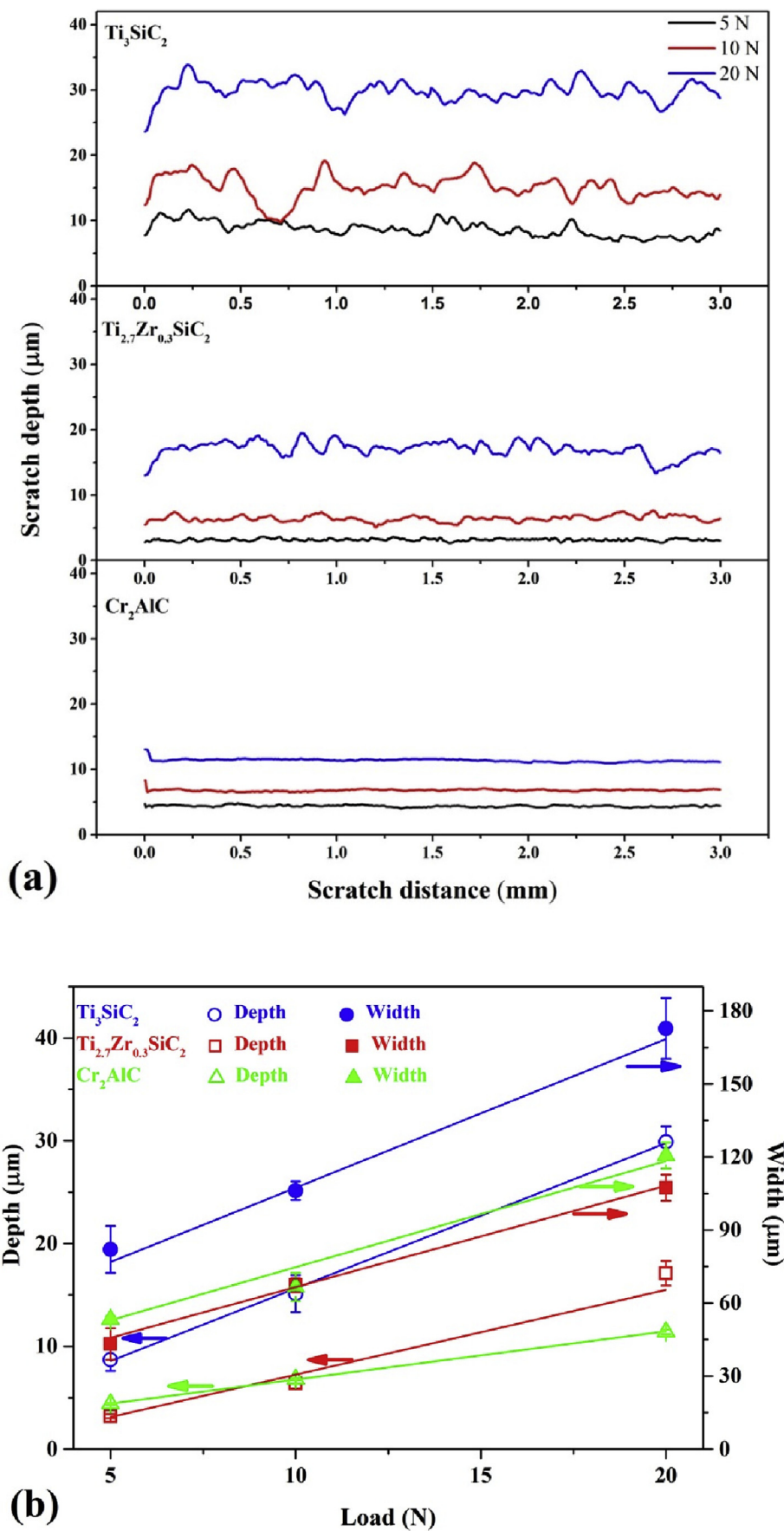| MAX Phase material	Second phase (vol%)	Grain size (μm)	Vickers hardness (GPa)
Ti_3SiC_2	2 (TiC)	Length: 41 ± 10 Width: 14 ± 4	2.8 ± 0.1 [28]
$Ti_{2.7}Zr_{0.3}SiC_2$	17 (TiC)	Length: 20 ± 7 Width: 6 ± 2	7.3 ± 0.2 [28]
Cr_2AlC	5 ($Cr_3C_7 + Cr_2C_3$)	21 ± 7	4.8 ± 0.8

Fig. 2. Scratch behavior of Ti$_3$SiC$_2$, Ti$_{2.7}$Zr$_{0.3}$SiC$_2$ and Cr$_2$AlC materials: (a) Scratch depth as a function of scratch distance, and (b) Scratch depth and width as a function of applied loads.
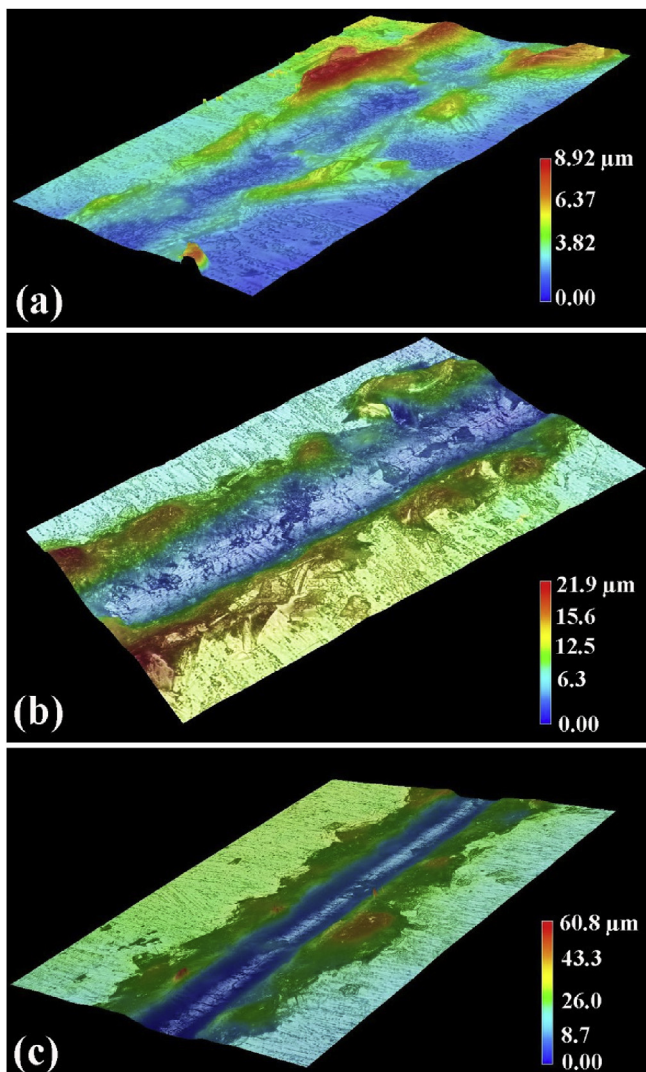
Fig. 3. 3D profiles of the scratch groove in Ti_3SiC_2 MAX phase material for different loads: (a) 5 N, (b) 10 N, and (c) 20 N.

$$W_r = \frac{V_w}{F_n \times S} \tag{1}$$

Where V_w is the volume of removed worn material, F_n is the applied load and S is the sliding distance. To determine the volume of worn material removed, a Keyence VHX-100 optical microscope (Osaka, Japan) was used to obtain a 3-D profile of the grooves produced.

The microhardness of the MAX phase materials was measured using a Zwick/Z2.5 hardness tester (Ulm, Germany) using a Vickers indenter and applying loads in the range of 1 to 100 N with a constant contact time of 10 s.

The phase composition was determined with X-Ray Diffraction (XRD) analysis using a Bruker D8 Advance diffractometer operated with Co-Kα radiation. The diffractograms were recorded in the 2θ range of 8 to 80° with a step size of 0.02° and a counting time per step of 1 s. These diffractograms were evaluated using the Bruker Diffrac EVA software (version 3).

The microstructure of the MAX phase samples before and after scratch testing was observed with scanning electron microscopy (SEM) using a JSM 6500F (JEOL, Japan). Grain size of MAX phase and volume fraction of the seconds phases was determined with image analysis using Image J software (version 1.49).

Table 2
Wear rate of MAX phase materials determined by scratch testing with different loads and comparison with other ceramics.

Materials	Loads (N)	Scratch depth (μm)	Scratch width (μm)	Wear rate ($\times 10^{-6}$ mm^3/Nm)	Ref.
Ti_3SiC_2	5	8.7 ± 1.1	82 ± 9.6	24 ± 2	This
	10	15.1 ± 1.8	106.2 ± 3.8	67 ± 8	work
	20	29.9 ± 1.5	172.8 ± 12.5	289 ± 16	
$Ti_{2.7}Zr_{0.3}SiC_2$	5	3.2 ± 0.2	43.1 ± 6.5	6.7 ± 0.8	This
	10	6.4 ± 0. 5	67.3 ± 2.9	13 ± 1	work
	20	17.1 ± 1.2	107.4 ± 5.8	28 ± 1	
Cr_2AlC	5	4.4 ± 0.1	53.2 ± 1.4	7.6 ± 0.6	This
	10	6.8 ± 0.1	66.6 ± 5.8	14 ± 1	work
	20	11.4 ± 0.2	120.6 ± 5.3	31 ± 1	
SiC-10 vol%Si	4	–	27.8–35.5	–	[27]
Al_2O_3	4	–	15.5–26.7	–	
Si_3N_4	4	–	10.0–28.2	–	
α-SiC	4	–	20.3–21.6	–	
Ti_2AlC coating	8	–	39–45	–	[27]

3. Results

3.1. Materials

The grains of the Ti_3SiC_2 and $Ti_{2.7}Zr_{0.3}SiC_2$ MAX phases have an elongated shape but there is no macroscopic preferred orientation of their long axis. The length and width of the Ti_3SiC_2 grains were 41 ± 10 μm and 14 ± 4 μm, respectively. The length and width of the $Ti_{2.7}Zr_{0.3}SiC_2$ grains were 20 ± 7 μm and 6 ± 2 μm, respectively, see Table 1. As shown in Table 1, the volume fraction of TiC impurities was 2% for the stoichiometric Ti_3SiC_2 material. For the solid solution strengthened material $Ti_{2.7}Zr_{0.3}SiC_2$, the TiC concentration increased to 17 vol% [28].

In the Cr_2AlC material, the grains are equiaxed with an average size of 21 ± 7 vol%. They contain about 5 vol% of two chromium carbides (viz. Cr_3C_7 and Cr_2C_3) as secondary phases. These chromium carbides are mainly distributed along the grain boundaries (see Fig. 1).

3.2. Scratch behavior

The scratch depth profiles of the MAX phase materials are shown in Fig. 2 for three applied loads 5, 10 and 20 N. For the Ti_3SiC_2 sample, the scratch depth fluctuated significantly over the tested distances for all applied loads; see Fig. 2(a). This indicates that Ti_3SiC_2 experienced locally varying deformation and cracking behavior, but at distances much larger than the size of the individual grains. Much less scratch depth fluctuations were observed in the scratch depth of $Ti_{2.7}Zr_{0.3}SiC_2$ and Cr_2AlC MAX phase materials; see Fig. 2 (a). A typical example of the scratch depth and scratch width profile of Ti_3SiC_2 created at the three different loads are shown in Fig. 3. It shows that the edges of the scratch track are relatively straight and that positions with a deeper local scratch depth show extensive upward extrusions outside the scratch track. Similar behavior has been found for the other two materials.

The average scratch depths and widths as a funtions of the load are plotted in Fig. 2(b) for the three MAX phase investigated. For all materials, the measured scratch depth and width increases linearly with the applied load. At loads of 5 and 10 N, comparable scratch depth and width values were recorded for the $Ti_{2.7}Zr_{0.3}SiC_2$ and Cr_2AlC materials. At a load of 20 N, the scratch depth for the $Ti_{2.7}Zr_{0.3}SiC_2$ material (17.1 ± 1.2 μm) is slightly larger than the that for the Cr_2AlC material (11.4 ± 0.2 μm). At any load, the scratch depth and width values for the Ti_3SiC_2 material are much larger (up to a factor 2) than those for $Ti_{2.7}Zr_{0.3}SiC_2$ and Cr_2AlC materials. The higher scratch depth and scratch width values for the Ti_3SiC_2 material result in much higher wear losses for this material than for the $Ti_{2.7}Zr_{0.3}SiC_2$ and Cr_2AlC materials;
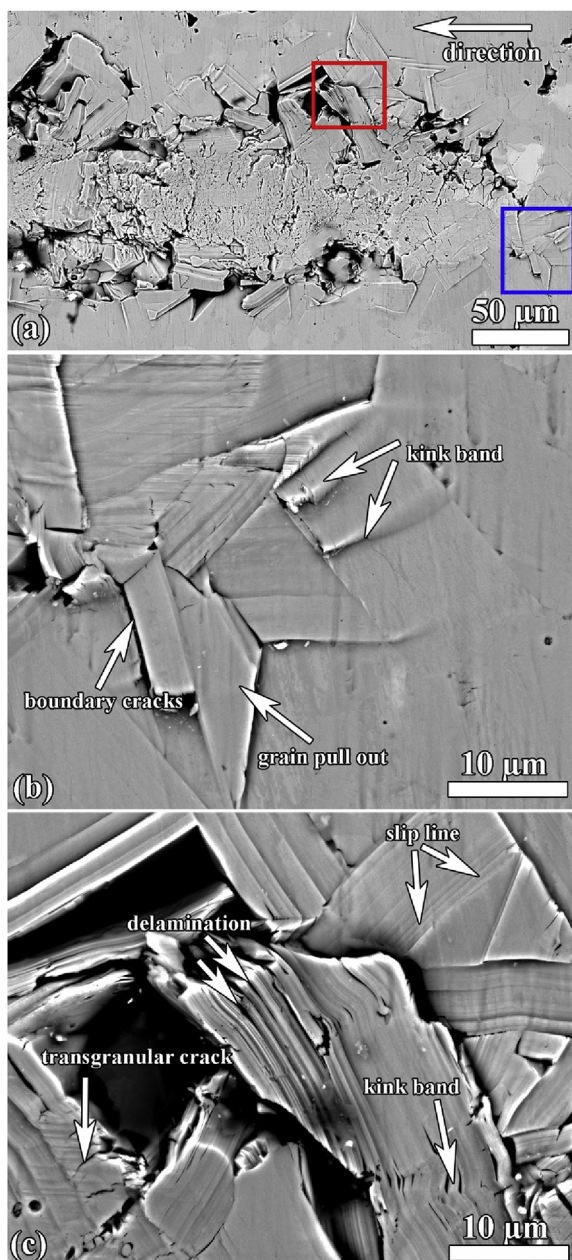
Fig. 4. Scratch damage of Ti$_3$SiC$_2$ MAX phase when applying a load of 5 N: (a) SEM secondary electron image, (b) enlargement corresponding to the white rectangle, and (c) enlargement corresponding to the black rectangle.

see Table 2. Finally, in the same Table the scratch depth values of the three materials are compared to similarly obtained values published in the literaturature for engineering ceramics (SiC, Si$_3$N$_4$ and Al$_2$O$_3$ and SiC with 10 vol% Si) and a Ti$_2$AlC coating. It is very clear that the scratch damage in these MAX phase materials is much more severe than that in the engineering ceramics. The relatively superior scratch resistance of the Ti$_2$AlC MAX phase coating material is attributed to the finer grain size.

3.3. Scratch damage observations

The top view of the microstructure of the Ti$_3$SiC$_2$ material after scratching with a load of 5 N is shown in Fig. 4. The micrograph shows a lot of plastic deformation and short local cracks. No larger and continuous cracks, such as partial cone cracks or radial cracks, commonly observed in scratch tracks for brittle ceramics [3,24,25] or glasses [26],
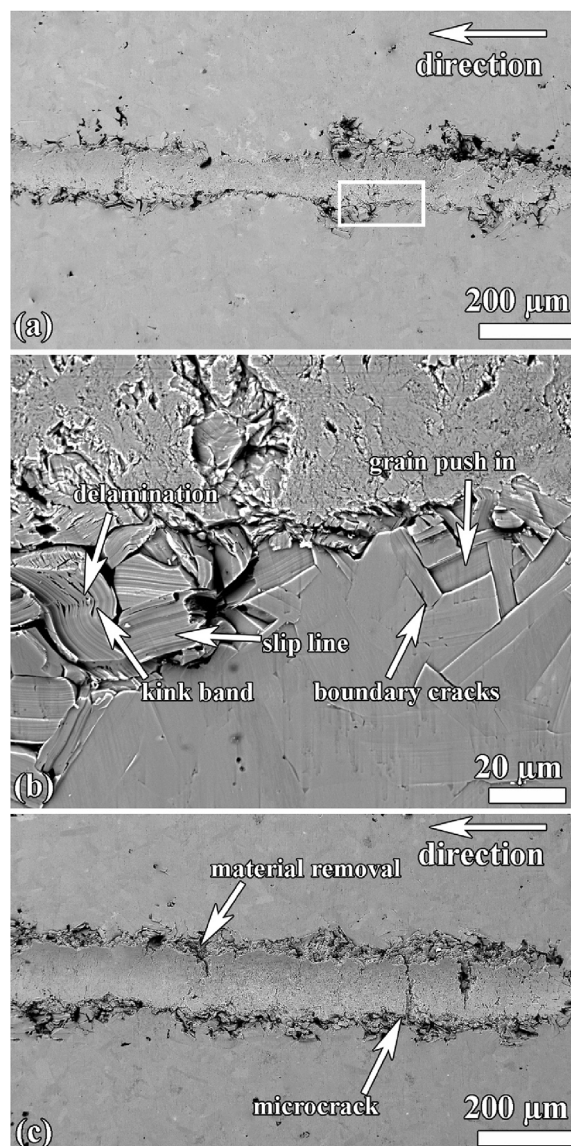

Fig. 5. Scratch damage of Ti$_3$SiC$_2$ MAX phase when applying a load of 10 and 20 N: (a) SEM secondary electron image for 10 N, (b) enlargement corresponding to the white rectangle, and (c) SEM secondary electron image for 20 N.

were observed. At the middle of scratch groove, delamination along the basal planes and micro-cracking perpendicular to the scratch direction was observed; see Fig. 4(b). At the edge of the scratch groove, "quasi-plastic" deformation (i.e. partly plastic and partly fracture, cf [29]) occurred by grain buckling, slip line, kink band formation and delamination, grain pull out and push in and boundary cracks; see Fig. 4(c) and (d). Such compound failure modes have frequently been observed in deformed or fractured MAX phases [30–32]. Also some cavities could be observed near the edge of the scratch groove. This is likely due to decohesion of grains during the scratch event, which ultimately leads to dislodgment of individual grains [24,33,34]. Similar scratch damage mechanisms were observed at a load of 10 N (Fig. 5(a) and (b)). However, at an applied load of 20 N, almost no "quasi-plastic" deformation was observed near the edge of the scratch groove; see Fig. 5(c). In contrast to ploughing, boundary cracking and material dislodgments leading to a large amount of material removal (see Table 2) were the dominant failure modes.

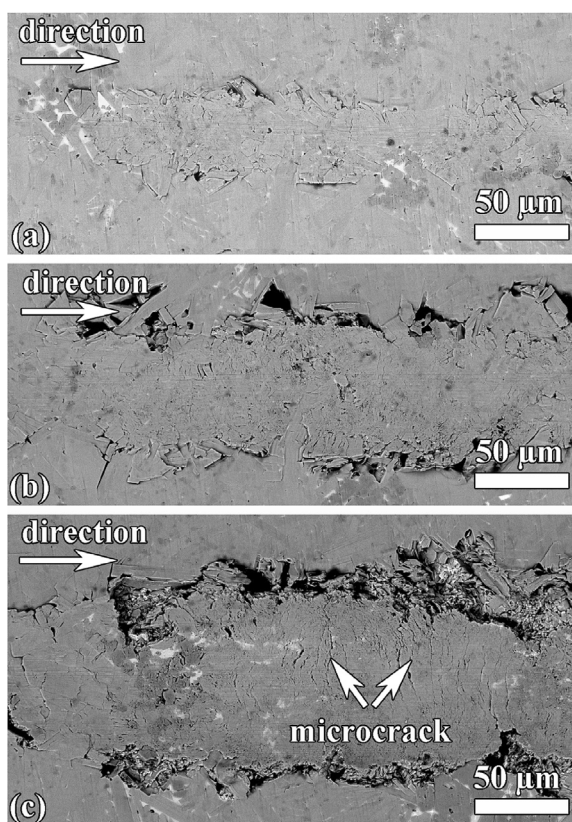In the Ti$_{2.7}$Zr$_{0.3}$SiC$_2$ MAX phase material, ploughing and boundary cracks formation were observed as the main wear mechanisms, while

Fig. 6. Scratch damage of $Ti_{2.7}Zr_{0.3}SiC_2$ MAX phase with different loads, SEM secondary electron image for: (a) 5 N, (b) 10 N, and (c) 20 N.

Fig. 7. Scratch damage of Cr_2AlC MAX phase with different loads, SEM secondary electron image for: (a) 5 N, (b) 10 N, and (c) 20 N.

almost no "quasi-plastic" deformation was observed (Fig. 6(a)) at a load of 5 N, When increasing the applied load up to 10 N, grain dislodgments, in addition to ploughing and boundary cracks, at the edge of the scratch groove took place; see Fig. 6(b). Upon further increasing the scratch load to 20 N, material removal by grain dislodgments became the dominant wear mechanism; see Fig. 6(c). Many micro-cracks perpendicular to the scratch direction formed in the middle of the scratch groove. No signs were observed which linked the wear pattern to the presence of 17 vol% of fine TiC carbides.

Lastly, in the Cr_2AlC MAX phase, the microstructure after scratching is very similar for all applied loads. In this case, ploughing is the dominant wear mechanism and grain boundary cracks and grain dislodgments occurred simultaneously; see Fig. 7. However, the scale of the damage was smaller than that observed in the $Ti_{2.7}Zr_{0.3}SiC_2$ material. No signs were observed which linked the wear pattern to the presence of the (5 vol %) chromium carbides.

4. Discussion

The microstructure of the MAX phase materials has significant impact on the deformation or material removal mechanisms upon scratching. In the almost pure Ti_3SiC_2 MAX phase having the largest grain size, "quasi-plastic" deformation behavior, such as grain buckling, kink band formation and grain delamination, slip lines, grain decohesion, grain boundary cracking, as well as transgranular fracture were observed when a scratch load of less than 10 N was applied; see Fig. 8. The deformation damage is similar to that observed after uniaxial compression of MAX phases [30–32,35]. The plastic deformation and kink band formation can either attribute to dislocation gliding along the basal plane of the hexagonal crystal lattice [36] or to incipient kink band (IKB) model by Barsoum [37]; see Fig. 8. To render the dislocation gliding on the basal plane of the hexagonal MAX phases to form kink
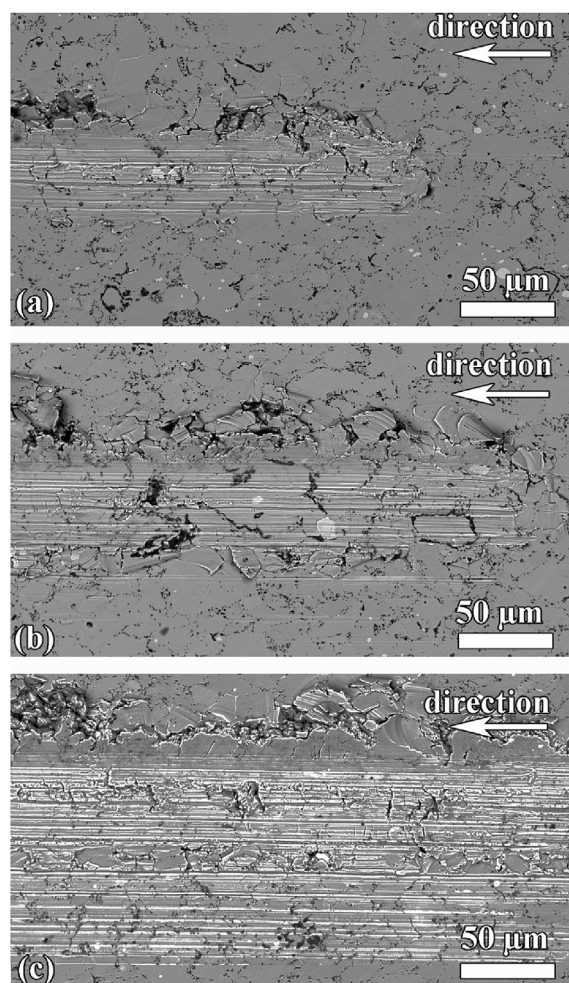
bands or ridges and grain delamination, a critical load generating a stress above a certain threshold should be applied. This threshold stress is a function of the grain size and follows the Hall-Petch relation [35,37]. For example, the threshold stress for fine grained Ti_3AlC_2 MAX phase (~10 μm in width) is about 244 MPa [31], while this threshold for coarse grained Ti_3AlC_2 (~25 μm in width) is about 125 MPa [32]. This rather strong grain size dependence could in part explain the larger plastic deformation in the Ti_3SiC_2 material than that in the $Ti_{2.7}Zr_{0.3}SiC_2$ and Cr_2AlC materials both having a grain size half that Ti_3SiC_2; see Table 1.

In a recent study [28], the effect of Ti substitution by Zr in Ti_3SiC_2 on the elastic and plastic properties of these solid solution strengthened materials has been studied in detail and the result confirm the increase in hardness due to the solid solution hardening effect of Zr while the elastic modulus remains more or less unchanged. However, it was observed that the increase in nano-hardness was significantly smaller than the Vickers hardness increase. So, part of the higher hardness of $Ti_{2.7}Zr_{0.3}SiC_2$ material is due to the material itself and part of it due to the finer grain size.

The hardness of the Cr_2AlC sample was lower than that of $Ti_{2.7}Zr_{0.3}SiC_2$ material while the grain sizes were more or less equal. As there is no contribution of solid solution hardening in Cr_2AlC, this lower hardness is to be expected. Recent work [38] on SPS produced Cr_2AlC material starting with fine or coarse powders has shown that there is no strong effect of grain size on hardness, but also showed that for finer grain sizes texture effects may have a beneficial effect on fracture toughness. The grain size of our material is in between two grain sizes
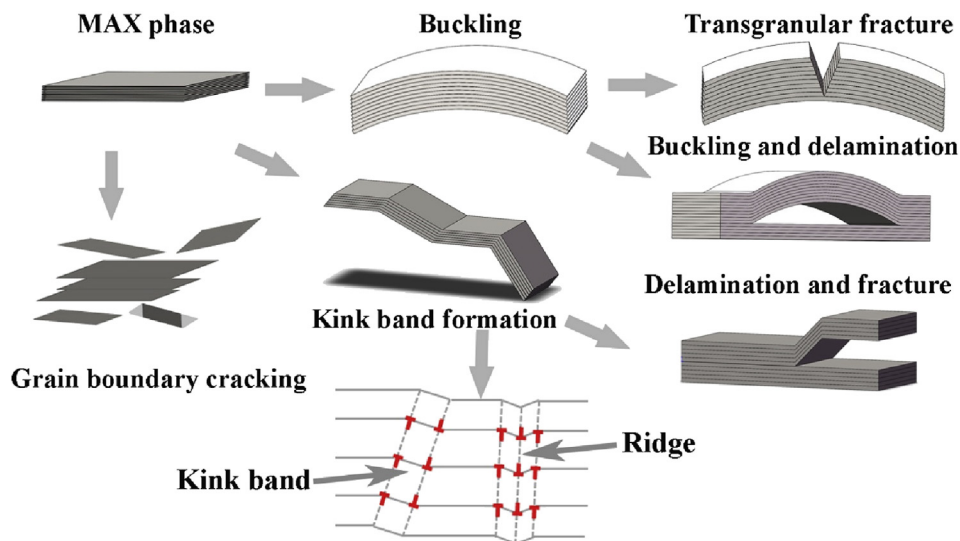
Fig. 8. Schematic of MAX phases deformation.

reported in [38] and this may indicate that some micro texture of [0001] plane could have been present. If so, the increase in fracture toughness would have a beneficial effect on the wear rate. More dedicated studies are required to establish a relationship between micro texture and wear rate in MAX phase materials.

5. Conclusions

Three different SPS produced MAX phases materials, viz.: Ti_3SiC_2, $Ti_{2.7}Zr_{0.3}SiC_2$ and Cr_2AlC were subjected to room temperature scratch tests at various loads to determine their abrasive wear behavior. The Ti_3SiC_2 material having the largest grain size has the lowest scratch resistance. The scratch resistance of $Ti_{2.7}Zr_{0.3}SiC_2$ and Cr_2AlC having a smaller grain size was significantly better and equal, not withstanding their different hardnesses.

The scratch damage mechanisms near the scratch grooves depends on the applied load and the microstructure. The soft coarse grained Ti_3SiC_2 showed "quasi-plastic" deformation behavior where grain bending, boundary cracks, kink band formation and delamination as well as transgranular fracture occur. On the other hand, the harder fine grained $Ti_{2.7}Zr_{0.3}SiC_2$ and Cr_2AlC materials showed deformation by ploughing, boundary cracks and materials dislodgments. The relatively good scratch resistance of Cr_2AlC may be due to micro texture effects.

References

[1] H. Czichos, D. Klaffke, E. Santner, M. Woydt, Advances in tribology: the materials point of view, Wear 190 (1995) 155–161 https://doi.org/10.1016/0043-1648(96)80014-7.

[2] P. Greil, Advanced engineering ceramics, Adv. Mater. 4 (2002) 709–716 https://doi.org/10.1002/1521-4095(20020517)14:10%3c709::AID-ADMA709%3e3.0.CO;2-9.

[3] R. Sivakumar, M.I. Jones, K. Hirao, W. Kanematsu, Scratch behavior of SiAlON ceramics, J. Eur. Ceram. Soc. 26 (2006) 351–359 https://doi.org/10.1016/j.jeurceramsoc.2004.11.010.

[4] S. van der Zwaag, Self Healing Materials an Alternative Approach to 20 Centuries of Materials Science, Springer, Dordrecht, 2007.

[5] G.P. Bei, B.J. Pedimonte, M. Pezoldt, J. Ast, T. Fey, M. Goeken, P. Greil, Crack healing in $Ti_2Al_{0.5}Sn_{0.5}C$–Al_2O_3 composites, J. Am. Ceram. Soc. 98 (2015) 1604–1610 https://doi.org/10.1111/jace.13496.

[6] T. Osada, K. Kamoda, M. Mitome, T. Hara, T. Abe, Y. Tamagawa, W. Nakao, T. Ohmura, A novel design approach for self-crack-healing structural ceramics with 3D networks of healing activator, Sci. Rep. 7 (2017) 17853 https://doi.org/10.1038/s41598-017-17942-6.

[7] M.W. Barsoum, The $M_{N+1}AX_N$ phases: a new class of solids thermodynamically stable nanolaminates, Prog. Solid State Chem. 28 (2000) 201–281 https://doi.org/10.1016/S0079-6786(00)00006-6.

[8] M.W. Barsoum, M. Radovic, Elastic and mechanical properties of the MAX phases, Annu. Rev. Mater. Res. 41 (2011) 195–227 https://doi.org/10.1146/annurev-matsci-062910-100448.

[9] X. Chen, G. Bei, Toughening Mechanisms in nanolayered MAX phase ceramics - a Review, Materials 10 (2017) 366 https://doi.org/10.3390/ma10040366.

[10] S. Li, G. Bei, X. Chen, L. Zhang, Y. Zhou, M. Mačković, E. Spiecker, P. Greil, Crack healing induced electrical and mechanical properties recovery in a Ti_2SnC ceramic, J. Eur. Ceram. Soc. 36 (1) (2016) 25–32 https://doi.org/10.1016/j.jeurceramsoc.2015.09.019.

[11] P. Greil, Generic principles of crack-healing ceramics, J. Adv. Ceram. 1 (2012) 249–267 https://doi.org/10.1007/s40145-012-0020-2.

[12] W.G. Sloof, R. Pei, S.A. McDonald, J.L. Fife, L. Shen, L. Boatemaa, A.-S. Farle, K. Yan, X. Zhang, S. van der Zwaag, P.D. Lee, P.J. Withers, Repeated crack healing in MAX-phase ceramics revealed by 4D in situ synchrotron X-ray tomographic microscopy, Sci. Rep. 6 (2016) 23040 https://doi.org/10.1038/srep23040.

[13] H.X. Zhai, Z.Y. Huang, M.X. Ai, Y. Zhou, Z.L. Zhang, S.B. Li, Tribophysical properties of polycrystalline bulk Ti_3AlC_2, J. Am. Ceram. Soc. 88 (2005) 3270–3274 https://doi.org/10.1111/j.1551-2916.2005.00588.x.

[14] Z. Huang, H. Zhai, M. Li, X. Liu, Y. Zhou, Friction behaviors and effects on current-carrying wear characteristics of bulk Ti_3AlC_2, Tribol. Trans. 57 (2014) 300–307 https://doi.org/10.1080/10402004.2013.871377.

[15] Z. Huang, H. Zhai, W. Zhou, X. Liu, M. Ai, Tribological behaviors and mechanisms of Ti_3AlC_2, Tribol. Lett. 27 (2007) 129–135 https://doi.org/10.1007/s11249-007-9202-4.

[16] L. Cai, Z. Huang, W. Hu, S. Hao, H. Zhai, Y. Zhou, Fabrication, mechanical properties, and tribological behaviors of Ti_2AlC and $Ti_2AlSn_{0.2}C$ solid solutions, J. Adv. Ceram. 6 (2017) 90–99 https://doi.org/10.1007/s40145-017-0221-9.

[17] Z. Huang, H. Xu, H. Zhai, Y. Wang, Y. Zhou, Strengthening and tribological surface self-adaptability of Ti_3AlC_2 by incorporation of Sn to form $Ti_3Al(Sn)C_2$ solid solutions, Ceram. Int. 41 (2015) 3701–3709 https://doi.org/10.1016/j.ceramint.2014.11.042.

[18] S. Wang, J. Cheng, S. Zhu, Z. Qiao, J. Yang, W. Liu, Frictional properties of Ti_3AlC_2 ceramic against different counterparts in deionized water and artificial seawater, Ceram. Int. 42 (2016) 4578–4585 https://doi.org/10.1016/j.ceramint.2015.11.153.

[19] S. Wang, S. Zhu, J. Cheng, Z. Qiao, J. Yang, W. Liu, Microstructural, mechanical and tribological properties of Al matrix composites reinforced with Cu coated Ti_3AlC_2, J. Alloy. Comp. 690 (2017) 612–620 https://doi.org/10.1016/j.jallcom.2016.08.175.

[20] J. Gonzalez-Julian, J. Llorente, M. Bram, M. Belmonte, O. Guillon, Novel Cr_2AlC MAX-phase/SiC fiber composites: synthesis, processing and tribological response, J. Eur. Ceram. Soc. 37 (2017) 467–475 https://doi.org/10.1016/j.jeurceramsoc.2016.09.029.

[21] S. Wang, J. Cheng, S. Zhu, Z. Qiao, J. Yang, W. Liu, Microstructure evolution, mechanical and tribological properties of $Ti_3(Al,Sn)C_2/Al_2O_3$ composites, J. Eur. Ceram. Soc. 38 (2018) 2502–2510 https://doi.org/10.1016/j.jeurceramsoc.2018.01.029.

[22] A. Loganathan, A. Sahu, C. Rudolf, C. Zhang, S. Rengifo, T. Laha, B. Boesl,

A. Agarwal, Multi-scale tribological and nanomechanical behavior of cold sprayed Ti$_2$AlC MAX phase coating, Surf. Coat. Technol. 334 (2018) 384–393 https://doi.org/10.1016/j.surfcoat. 2017.11.067.

[23] G. Subhash, R. Bandyo, A new scratch resistance measure for structural ceramics, J. Am. Ceram. Soc. 88 (2005) 918–925 https://doi.org/10.1111/j.1551-2916.2005.00181.x.

[24] H.H.K. Xu, N.P. Padture, S. Jahanmir, Effect of microstructure on material-removal mechanisms and damage tolerance in abrasive machining of silicon carbide, J. Am. Ceram. Soc. 78 (9) (1995) 2443–2448 https://doi.org/10.1111/j.1151-2916.1995.tb08683.x.

[25] S. Kun Lee, R. Tandon, M.J. Readey, B.R. Lawn, Scratch damage in zirconia ceramics, J. Am. Ceram. Soc. 83 (6) (2000) 1428–1432 https://doi.org/10.1111/j.1151-2916.2000. tb01406.x.

[26] F. Petit, C. Ott, F. Cambier, Multiple scratch tests and surface-related fatigue properties of monolithic ceramics and soda lime glass, J. Eur. Ceram. Soc. 29 (2009) 1299–1307 https://doi.org/10.1016/j.jeurceramsoc.2008.09.019.

[27] M.G. Gee, Low load multiple scratch tests of ceramics and hard metals, Wear 250 (2001) 264–281 https://doi.org/10.1016/S0043-1648(01)00591-9.

[28] L. Qu, G. Bei, B. Stelzer, H. Rueß, J.M. Schneider, D. Cao, S. van der Zwaag, W.G. Sloof, Synthesis, crystal structure, microstructure and mechanical properties of (Ti$_{1-x}$Zr$_x$)$_3$SiC$_2$ MAX phase solid solutions, Ceram. Int. 45 (2019) 1400–1480 https://doi.org/10.1016/j. ceramint.2018.10.030.

[29] M.W. Barsoum, T. El-Raghy, Room temperature ductile carbides, Metall. Mater. Trans. A 30 (1999) 363–369 https://doi.org/10.1007/s11661-999-0325-0.

[30] M.W. Barsoum, T. Zhen, S. Kalidindi, M. Radovic, A. Murugaiah, Fully reversible, dislocation-based compressive deformation of Ti$_3$SiC$_2$ up to 1 GPa, Nat. Mater. 2 (2003) 107–111 https://doi.org/10.1038/nmat814.

[31] A.G. Zhou, M.W. Barsoum, Kinking nonlinear elastic deformation of Ti$_3$AlC$_2$, Ti$_2$AlC, Ti$_3$Al(C$_{0.5}$,N$_{0.5}$)$_2$ and Ti$_2$Al(C$_{0.5}$,N$_{0.5}$), J. Alloy. Comp. 498 (2010) 62–70 https://doi.org/10.1016/j.jallcom.2010.03.099.

[32] G.P. Bei, G. Laplanche, V. Gauthier, J. Bonneville, S. Dubois, Compressive behavior of Ti$_3$AlC$_2$ and Ti$_3$Al$_{0.8}$Sn$_{0.2}$C$_2$ MAX phases at room temperature, J. Am. Ceram. Soc. 96 (2013) 567–576 https://doi.org/10.1111/jace.12092.

[33] H.H.K. Xu, S. Jahanmir, Microfracture and material removal in scratching of alumina, J. Mater. Sci. 30 (1995) 2235–2247 https://doi.org/10.1007/BF01184566.

[34] H.H.K. Xu, S. Jahanmir, Y. Wang, Effect of grain size on scratch interactions and material removal in alumina, J. Am. Ceram. Soc. 78 (1995) 881–891 https://doi.org/10.1111/j.1151-2916.1995.tb08409.x.

[35] M.W. Barsoum, S. Basu, Kinking nonlinear elastic solids, Encyclopedia of Materials: Science and Technology, Elsevier, Oxford, 2010, pp. 1–23 https://doi.org/10.1016/B978-008043152-9.02245-4.

[36] J.B. Hess, C.S. Barrett, Structure and nature of kink bands in zinc, JOM (J. Occup. Med.) 1 (1949) 599–606 https://doi.org/10.1007/BF03398902.

[37] M.W. Barsoum, T. Zhen, A. Zhou, S. Basu, S.R. Kalidindi, Microscale modeling of kinking nonlinear elastic solids, Phys. Rev. B Condens. Matter Mater. Phys. 71 (2005) 134101-1 - 134101-8 https://doi.org/10.1103/PhysRevB.71.134101.